

Temporary velocity correction-based immersed boundary–lattice Boltzmann method for incompressible flows in porous media at representative elementary volume scale

Cite as: Phys. Fluids **34**, 043110 (2022); <https://doi.org/10.1063/5.0087342>

Submitted: 04 February 2022 • Accepted: 03 April 2022 • Published Online: 21 April 2022

Xiang Liu (刘翔),  Zi-Xiang Tong (童自翔) and Ya-Ling He (何雅玲)



View Online



Export Citation



CrossMark

ARTICLES YOU MAY BE INTERESTED IN

[A lattice Boltzmann study on the bouncing behavior of equal-sized droplet collision](#)

Physics of Fluids **34**, 043318 (2022); <https://doi.org/10.1063/5.0087964>

[A hybrid scheme coupling lattice Boltzmann method and finite-volume lattice Boltzmann method for steady incompressible flows](#)

Physics of Fluids **34**, 037114 (2022); <https://doi.org/10.1063/5.0085370>

[Investigation of bubble dynamics in a micro-channel with obstacles using a conservative phase-field lattice Boltzmann method](#)

Physics of Fluids **34**, 043312 (2022); <https://doi.org/10.1063/5.0085217>

APL Machine Learning

Open, quality research for the networking communities

Now Open for Submissions

LEARN MORE



Temporary velocity correction-based immersed boundary–lattice Boltzmann method for incompressible flows in porous media at representative elementary volume scale

Cite as: Phys. Fluids **34**, 043110 (2022); doi: 10.1063/5.0087342

Submitted: 4 February 2022 · Accepted: 3 April 2022 ·

Published Online: 21 April 2022




View Online



Export Citation



CrossMark

Xiang Liu (刘翔),¹ Zi-Xiang Tong (童自翔),^{2,a)}  and Ya-Ling He (何雅玲)¹

AFFILIATIONS

¹Key Laboratory of Thermo-Fluid Science and Engineering of Ministry of Education, School of Energy and Power Engineering, Xi'an Jiaotong University, Xi'an, Shaanxi 710049, China

²School of Human Settlements and Civil Engineering, Xi'an Jiaotong University, Xi'an, Shaanxi 710049, China

^{a)}Author to whom correspondence should be addressed: zxtong@xjtu.edu.cn

ABSTRACT

The immersed boundary (IB)–lattice Boltzmann (LB) method is an effective strategy for complex boundary condition treatment. By adding an extra body force term in the LB equation properly, the specific velocity boundary condition can be enforced in this method. However, when it comes to incompressible flows through porous media at the representative elementary volume (REV) scale, the conventional IB–LB method fails because the velocity and the force term induced by porous media are coupled. In order to solve this problem, a temporary velocity is used to construct the IB-induced force term with the enforcement of the velocity boundary condition. The temporary velocity is decomposed into the intermediate temporary velocity and the corresponding correction. By this treatment, the temporary velocity correction is the linear function of the IB-induced force term. Furthermore, to obtain the force term accounting for the IB, the velocity boundary condition is transformed to the temporary velocity. Consequently, a temporary velocity correction-based IB–LB method is established for the incompressible flows at the REV scale. To avoid the error of explicitly calculating the IB-induced force term, the multi-direct-forcing scheme is employed in which iteration is carried out in terms of the specific boundary condition. The proposed IB–LB method for REV-scale incompressible flows is applied for the Couette flow in a porous annulus and lid driven flow in a square cavity filled with porous matrix. Numerical results show the computational accuracy of the developed IB–LB method.

Published under an exclusive license by AIP Publishing. <https://doi.org/10.1063/5.0087342>

I. INTRODUCTION

Incompressible flows inside complex geometry filled with porous media are widely encountered in scientific research and engineering applications, such as building energy technologies, utilization of shale gas, and energy storage processes.^{1–3} Numerical research can effectively increase the understanding of these practical processes. There are two popular approaches to describe this phenomenon: the representative elementary volume (REV)-scale approach and the pore-scale approach.⁴ Compared with the pore-scale approach, the REV-scale approach is based on volume-averaged conservation equations, and different force terms are employed to represent the effect of porous media. The detailed geometric information of the porous matrix is expressed by effective parameters, and the computational scale can be enlarged. Due to its simplicity and efficiency, numerical investigations

based on the REV-scale approach are widely conducted for fluid flows through porous media.^{5,6}

The lattice Boltzmann (LB) method has become a useful strategy for complex fluid flows and heat transfer simulations in the past 30 years. It is a special difference form of discrete velocity Boltzmann equation along the characteristic line. Due to its clear kinetic background, the discretization of nonlinear and nonlocal convection term in traditional macroscopic numerical methods can be replaced by the local collision and linear streaming of the density distribution function.^{7–10} Additionally, the LB method has advantages on the implementation of boundary condition and parallelism. In view of these advantages, several LB models based on different semi-empirical models for the REV-scale incompressible flows are established.^{11–14}

Furthermore, the boundary condition should be emphasized for incompressible fluid flows in porous media with a complex geometry. Among different boundary condition schemes in the field of computational fluid dynamics, the immersed boundary (IB) method becomes an attractive method because the boundary condition is transformed to a body force term without heavily works on the generation of body conformal grid.¹⁵ In the IB method, a set of Lagrangian grid (consisted by a group of IB points) is used to represent the effect of IB, and the surface force is introduced to the IB to enforce the specific boundary condition. The macroscopic variables on different grid should be converted. The specific velocity condition on the IB is interpolated by velocity on the Eulerian grid, while the surface force term on the IB is spread to the IB-related body force term on the Eulerian grid.¹⁵ Both the LB method and IB method are employed on the uniform Eulerian grid. Thus, it is promising to make a combination of these two methods, and several paper research show that the IB-LB method is an effective numerical method for the implementation of complex boundary condition.^{16,17}

The early IB-LB method was proposed by Feng and Michaelides.¹⁶ By employing an artificial spring parameter to consider the fictitiously tiny deformation of the IB, the penalty scheme is employed to obtain the force on IB points. However, the artificial spring parameter can significantly affect the numerical results. To overcome this drawback, another direct-forcing IB-LB method is proposed.¹⁸ The force term induced by the IB is calculated by the explicit discretization of momentum equation. Subsequently, by evaluating the IB-induced force term through the momentum exchange of density distribution functions, Niu *et al.*¹⁹ developed a novel IB-LB method, and the simplicity merit of LB method is maintained. Note that the IB effect is exerted by discrete force term in the LB equation, different force schemes can influence the entire accuracy. The discrete force term schemes can be mainly classified as the lumped-forcing method^{20,21} and split-forcing method.^{22,23} The IB-LB method used in Refs. 16 and 18 employed the lumped-forcing method in which the effect of force term is only considered in the collision process of density distribution functions. However, the discrete lattice effects exist, which can affect the overall numerical accuracy in the lumped-forcing method. To overcome this weakness, the split-forcing method is widely used in the LB equations. The force term not only participates in the collision but also corrects the velocity in the macroscopic quantities calculation. As reported by Wu and Shu,²⁴ the calculation of the force term is implicit because the velocity on the IB will be influenced after correcting the velocity on the Lagrangian grid. Thus, the velocity boundary condition cannot be accurately guaranteed through pre-computed force. The force term and correction of velocity should be solved simultaneously. Based on this idea, taking the velocity correction as unknown, an implicit IB-LB method on IB points is constructed to enforce the specific velocity. Subsequently, Kang and Hassan¹⁷ proposed a multi-direct-forcing IB-LB method. Compared with the implicit correction IB-LB method, the IB-induced force term is solved iteratively to satisfy the velocity on the IB without matrix manipulations.

However, current IB-LB methods mainly focus on the flows without porous media in which the relation between IB-related force term and velocity correction is linear (referred to as the conventional IB-LB methods in the rest of the paper). As a result, the IB-induced force term is obtained through the velocity correction on the IB, and

velocity is corrected directly vice versa. When it comes to REV-scale incompressible flows in porous media, the force term accounting for the effect of porous media couples with the velocity, such as the Darcy term, Brinkman term, and Forchheimer term.⁴ Therefore, the linear relation between velocity correction and the IB-induced force term in the conventional IB-LB method cannot be established. The IB-induced force term is hard to be directly obtained, and the velocity correction on the Eulerian grid is unknown. To overcome this problem, a temporary velocity is introduced to derive the velocity and IB-induced force term in this work. By using the temporary velocity, the linear relation between the temporary velocity and IB-induced force term is established. Different with the conventional IB-LB method, the boundary condition of velocity is converted to temporary velocity, and the linear relation between temporary velocity-correction and IB-induced force term is established to decouple the velocity and force term. Therefore, the temporary velocity correction-based IB-LB for the REV-scale flows in porous media is proposed. Additionally, the multi-direct-forcing method is employed to guarantee the velocity boundary condition accurately.

In the current work, the temporary velocity correction-based IB-LB method for the fluid flows through porous media is illustrated. Section II gives the governing equations and the detailed derivation of the proposed REV-scale IB-LB method. Section III verifies the proposed IB-LB method by the Couette flow in a porous annulus and lid driven flow in a cavity filled with porous matrix. Last, Sec. IV draws some conclusions of this work.

II. NUMERICAL METHOD

A. Governing equations

Assuming the porous media is homogeneous and isotropic, and ignoring porous matrix deformation, the REV-scale governing equations for the incompressible and laminar flow through porous media with an IB are given by^{15,25}

$$\nabla \cdot \mathbf{u} = 0, \quad (1)$$

$$\frac{\partial \mathbf{u}}{\partial t} + \mathbf{u} \cdot \nabla \left(\frac{\mathbf{u}}{\varepsilon} \right) = -\frac{1}{\rho} \nabla(\varepsilon p) + \nu_e \nabla \cdot [\nabla \mathbf{u} + (\nabla \mathbf{u})^T] + \mathbf{F}_b + \mathbf{F}_s, \quad (2)$$

$$\mathbf{F}_s(\mathbf{x}, t) = \int_{\Gamma} \mathbf{f}_s(s, t) \delta[\mathbf{x} - \mathbf{X}(s, t)] ds, \quad (3)$$

$$\mathbf{u}[\mathbf{X}(s, t), t] = \int_{\Omega} \mathbf{u}(\mathbf{x}, t) \delta[\mathbf{x} - \mathbf{X}(s, t)] d\mathbf{x}, \quad (4)$$

where ρ , p , and \mathbf{u} are the density, volume-averaged pressure, and velocity, respectively, ε is the porosity, ν_e is the effective kinematic viscosity, and \mathbf{F}_b is the body force term accounting for the effect of porous media. The body force \mathbf{F}_s is introduced to mimic the effect of IB, and \mathbf{f}_s is the surface force on the IB. Γ and Ω stand for the IB and fluid domains, respectively. s and \mathbf{x} represent the Lagrangian and Eulerian coordinates, respectively, t denotes the time, $\mathbf{X}(s, t)$ is the corresponding Eulerian coordinate of s , and $\delta[\mathbf{x} - \mathbf{X}(s, t)]$ is the Dirac delta function. The force term \mathbf{F}_b can be expressed as

$$\mathbf{F}_b(\mathbf{x}, t) = \mathbf{F}_b[\mathbf{u}(\mathbf{x}, t)] = -\frac{\varepsilon \nu}{K} \mathbf{u} - \frac{\varepsilon F_e}{\sqrt{K}} |\mathbf{u}| \mathbf{u}, \quad (5)$$

where ν and K are the kinematic viscosity and permeability, respectively. The Forchheimer coefficient F_e is given by²⁶

$$F_e = \frac{1.75}{\sqrt{150\varepsilon^3}}. \quad (6)$$

The dimensionless parameters used to characterize flows are Reynolds number (Re), Darcy number (Da), and viscosity ratio (J), which can be defined as⁴

$$Re = \frac{L_c u_c}{\nu}, \quad Da = \frac{K}{L_c^2}, \quad J = \frac{\nu_e}{\nu}, \quad (7)$$

where u_c and L_c are the characteristic velocity and length, respectively.

B. REV-scale IB-LB method

The REV-scale incompressible velocity field is solved by an LB equation with a single-relaxation-time collision term, which can be expressed as¹¹

$$f_i(\mathbf{x} + \mathbf{e}_i \delta_t, t + \delta_t) - f_i(\mathbf{x}, t) = -\frac{1}{\tau} [f_i(\mathbf{x}, t) - f_i^{\text{eq}}(\mathbf{x}, t)] + \delta_t F_i, \quad (8)$$

where $f_i(\mathbf{x}, t)$ is the density distribution function, δ_t is the lattice time step, τ is the dimensionless relaxation time, and F_i is the discrete force term. For two-dimensional problems in this work, the two-dimensional nine-velocity (D2Q9) model is employed in which the lattice velocity \mathbf{e}_i is defined as²⁷

$$\mathbf{e}_i = \begin{cases} (0, 0), & i = 0, \\ c(\cos[(i-1)\pi/2], \sin[(i-1)\pi/2]), & i = 1-4, \\ \sqrt{2}c(\cos[(2i-9)\pi/4], \sin[(2i-9)\pi/4]), & i = 5-8, \end{cases} \quad (9)$$

where the lattice constant $c = \delta_x/\delta_t$, and δ_x is the lattice space.

The equilibrium distribution function f_i^{eq} can be expressed as¹¹

$$f_i^{\text{eq}}(\mathbf{x}, t) = \omega_i \rho \left[1 + \frac{\mathbf{e}_i \cdot \mathbf{u}}{c_s^2} + \frac{(\mathbf{e}_i \cdot \mathbf{u})^2}{2\varepsilon c_s^4} - \frac{\mathbf{u}^2}{2\varepsilon c_s^2} \right], \quad (10)$$

where ω_i is the weight and c_s is the lattice sound speed. For the D2Q9 model, $\omega_0 = 4/9$, $\omega_{1-4} = 1/9$, $\omega_{5-8} = 1/36$, and $c_s = c/\sqrt{3}$.

To eliminate the discrete lattice effects, the split-forcing method developed in Ref. 22 is employed. The discrete force term F_i is given by¹¹

$$F_i = \omega_i \rho \left(1 - \frac{1}{2\tau} \right) \left[\frac{\mathbf{e}_i \cdot (\mathbf{F}_s + \mathbf{F}_b)}{c_s^2} + \frac{\mathbf{u}(\mathbf{F}_s + \mathbf{F}_b) : (\mathbf{e}_i \mathbf{e}_i - c_s^2 \mathbf{I})}{\varepsilon c_s^4} \right]. \quad (11)$$

The relation between effective viscosity ν_e and dimensionless relaxation time τ is given by

$$\nu_e = c_s^2 \delta_t (\tau - 0.5). \quad (12)$$

The macroscopic velocity \mathbf{u} and density ρ can be calculated by

$$\rho(\mathbf{x}, t) = \sum_i f_i(\mathbf{x}, t), \quad (13)$$

$$\mathbf{u}(\mathbf{x}, t) = \frac{1}{\rho(\mathbf{x}, t)} \sum_i \mathbf{e}_i f_i(\mathbf{x}, t) + \frac{\delta_t}{2} \{ \mathbf{F}_b[\mathbf{u}(\mathbf{x}, t)] + \mathbf{F}_s(\mathbf{x}, t) \}. \quad (14)$$

Because the force term \mathbf{F}_b is determined by a quadratic function of velocity \mathbf{u} , as shown in Eq. (5), a temporary velocity \mathbf{v} is introduced to explicitly calculate \mathbf{u} as¹¹

$$\mathbf{v}(\mathbf{x}, t) = \mathbf{u}(\mathbf{x}, t) - \frac{\delta_t}{2} \mathbf{F}_b[\mathbf{u}(\mathbf{x}, t)] = \frac{1}{\rho(\mathbf{x}, t)} \sum_i \mathbf{e}_i f_i(\mathbf{x}, t) + \frac{\delta_t}{2} \mathbf{F}_s(\mathbf{x}, t), \quad (15)$$

$$\mathbf{u}(\mathbf{x}, t) = \frac{\mathbf{v}(\mathbf{x}, t)}{c_0 + \sqrt{c_0^2 + c_1 |\mathbf{v}(\mathbf{x}, t)|}}, \quad (16)$$

$$\mathbf{v}(\mathbf{x}, t) = [2c_0 + c_1 |\mathbf{u}(\mathbf{x}, t)|] \mathbf{u}(\mathbf{x}, t), \quad (17)$$

where $c_0 = \frac{1}{2} \left(1 + \varepsilon \frac{\delta_t \nu}{2K} \right)$, $c_1 = \varepsilon \frac{\delta_t F_e}{2\sqrt{K}}$, and $p = \rho c_s^2 / \varepsilon$.

Figure 1 shows the details of the IB-LB method. Both Eulerian grid and Lagrangian grid are employed. By employing a discrete delta function $D(\mathbf{x})$, Eqs. (3) and (4) can be discretized as^{15,25}

$$\mathbf{F}_s(\mathbf{x}, t) = \sum_j \mathbf{f}_s(s_j, t) D(\mathbf{x} - \mathbf{X}_j) \Delta s_j, \quad (18)$$

$$\mathbf{u}(\mathbf{X}_j, t) = \sum_{\mathbf{x}} \mathbf{u}(\mathbf{x}, t) D(\mathbf{x} - \mathbf{X}_j) \delta_x^2, \quad (19)$$

where \mathbf{X}_j is the Eulerian coordinate of the j th Lagrangian point s_j ($j = 1, 2, \dots, N$), and Δs_j is the corresponding IB length of the IB point s_j .

The $D(\mathbf{x})$ can be expressed as²⁸

$$D(\mathbf{x}) = \frac{1}{\delta_x^2} d\left(\frac{x}{\delta_x}\right) d\left(\frac{y}{\delta_x}\right), \quad (20)$$

where $\mathbf{x} = (x, y)$ for two-dimensional problems. The detailed form of $d(x)$ can be given by²⁸

$$d(x) = \begin{cases} \frac{1}{8} \left(3 - 2|x| + \sqrt{1 + 4|x| - 4|x|^2} \right), & |x| < 1, \\ \frac{1}{8} \left(5 - 2|x| - \sqrt{-7 + 12|x| - 4|x|^2} \right), & |x| < 2, \\ 0, & |x| \geq 2. \end{cases} \quad (21)$$

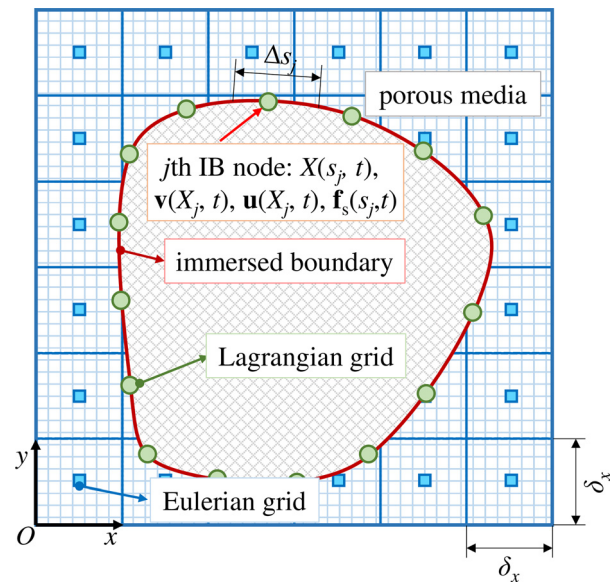


FIG. 1. The schematic diagram of the IB-LB method.

In order to explain the proposed REV-scale IB-LB method clearly, the conventional IB-LB method, which is the IB-LB method for flows without porous media, is briefly described as below. When neglecting the effect of porous media, namely, $\varepsilon \rightarrow 1$ and $K \rightarrow \infty$ ($\mathbf{F}_b[\mathbf{u}(\mathbf{x}, t)] = 0$), velocity $\mathbf{u}(\mathbf{x}, t)$ can be decomposed into two parts, intermediate velocity $\mathbf{u}^*(\mathbf{x}, t)$ and velocity correction $\delta\mathbf{u}(\mathbf{x}, t)$, which are given as¹⁷

$$\begin{aligned}\mathbf{u}(\mathbf{x}, t) &= \mathbf{u}^*(\mathbf{x}, t) + \delta\mathbf{u}(\mathbf{x}, t), \\ \mathbf{u}^*(\mathbf{x}, t) &= \frac{1}{\rho(\mathbf{x}, t)} \sum_i \mathbf{e}_i f_i(\mathbf{x}, t) = \frac{\delta_t}{2} \mathbf{F}_s(\mathbf{x}, t).\end{aligned}\quad (22)$$

The $\mathbf{u}^*(\mathbf{x}, t)$ can be determined by post-streaming density distribution functions $f_i(\mathbf{x}, t)$. The relation between $\delta\mathbf{u}(\mathbf{x}, t)$ and $\mathbf{F}_s(\mathbf{x}, t)$ is linear, thus $\mathbf{F}_s(\mathbf{x}, t)$ can be used to directly calculate $\delta\mathbf{u}(\mathbf{x}, t)$ and correct $\mathbf{u}(\mathbf{x}, t)$.

The main issue of the conventional IB-LB method is to obtain the unknown surface force term $\mathbf{f}_s(s_j, t)$ on the IB, which will be spread to the body force term $\mathbf{F}_s(\mathbf{x}, t)$ on the Eulerian grid through Eq. (18). To represent the effect of the IB, the $\mathbf{F}_s(\mathbf{x}, t)$ is employed in both the collision process of $f_i(\mathbf{x}, t)$ and the correction of $\mathbf{u}^*(\mathbf{x}, t)$ through Eq. (22). The specified velocity boundary condition $\mathbf{u}(\mathbf{X}_j, t)$ on the IB should be satisfied by interpolating the corrected velocity $\mathbf{u}(\mathbf{x}, t)$ on the Eulerian grid based on Eq. (19).

In the conventional IB-LB method, based on the linearity between $\delta\mathbf{u}(\mathbf{x}, t)$ and $\mathbf{F}_s(\mathbf{x}, t)$ in Eq. (22), the body force term $\mathbf{F}_s(\mathbf{X}_j, t)$ on the IB is calculated as

$$\mathbf{F}_s(\mathbf{X}_j, t) = \frac{2}{\delta_t} [\mathbf{u}(\mathbf{X}_j, t) - \mathbf{u}^*(\mathbf{X}_j, t)], \quad (23)$$

where the $\mathbf{u}(\mathbf{X}_j, t)$ is the specific velocity of the j th IB point. Based on Eq. (19), the corresponding intermediate velocity $\mathbf{u}^*(\mathbf{X}_j, t)$ is interpolated from $\mathbf{u}^*(\mathbf{x}_j, t)$ by

$$\mathbf{u}^*(\mathbf{X}_j, t) = \sum_{\mathbf{x}} \mathbf{u}^*(\mathbf{x}, t) D(\mathbf{X}_j - \mathbf{x}) \delta_{\mathbf{x}}^2. \quad (24)$$

In the direct-forcing IB-LB method, the surface force term $\mathbf{f}_s(s_j, t)$ is given by^{17,29}

$$\mathbf{f}_s(s_j, t) = \delta_{\mathbf{x}} \mathbf{F}_s(\mathbf{X}_j, t). \quad (25)$$

The $\mathbf{f}_s(s_j, t)$ is spread to the Eulerian grid using Eq. (18) to obtain the $\mathbf{F}_s(\mathbf{x}, t)$. Then, the $\mathbf{F}_s(\mathbf{x}, t)$ is used in the evolution equation for fluid flow, and the intermediate velocity $\mathbf{u}^*(\mathbf{x}, t)$ can be corrected through Eq. (22).

In essence, when the velocities $\mathbf{u}(\mathbf{X}_j, t)$ on the IB are specified by velocity boundary conditions, Eqs. (18), (19), and (22) construct a linear equation system for solving unknown $\mathbf{f}_s(s_j, t)$. The $\mathbf{f}_s(s_j, t)$ on all IB points should be solved simultaneously through matrix manipulation.²⁴ From this point of view, the aforementioned procedures in the direct-forcing IB-LB can be only regarded as a single iteration step in solving the linear equation. The velocity on the IB, which is interpolated from the corrected velocity $\mathbf{u}(\mathbf{x}, t)$ with the explicitly calculated $\mathbf{f}_s(s_j, t)$ through Eq. (23), will deviate the specific velocity.²⁴ It is not sufficient to enforce the specific boundary condition on the IB.

To overcome this drawback, the multi-direct-forcing method¹⁷ can be used to enforce the specific boundary condition. In this method, $\mathbf{f}_s(s_j, t)$ is solved iteratively until the specific velocity on the IB is obtained. On the IB point s_j , $\mathbf{f}_s(s_j, t)$ can be calculated by^{17,29}

$$\mathbf{f}_s^n(s_j, t) = \delta_{\mathbf{x}} \mathbf{F}_s^n(\mathbf{X}_j, t) = 2\delta_{\mathbf{x}} \frac{\mathbf{u}(\mathbf{X}_j, t) - \mathbf{u}^{*,n-1}(\mathbf{X}_j, t)}{\delta_t}, \quad (26)$$

where the subscript n stands for the iteration level. The $\mathbf{u}^{*,n}(\mathbf{X}_j, t)$ is interpolated from $\mathbf{u}^{*,n}(\mathbf{x}, t)$, which is given by

$$\mathbf{u}^{*,n}(\mathbf{x}, t) = \mathbf{u}^{*,n-1}(\mathbf{x}, t) + \frac{1}{2} \delta_t \mathbf{F}_s^n(\mathbf{x}, t). \quad (27)$$

The force term $\mathbf{F}_s^n(\mathbf{x}, t)$ is obtained through Eq. (18) from $\mathbf{f}_s^n(s_j, t)$. The iteration will be stopped until $\mathbf{u}^{*,n}(\mathbf{X}_j, t)$ converges to the specific boundary condition $\mathbf{u}(\mathbf{X}_j, t)$ or n reaches a pre-defined maximum iteration number n_{\max} . The $\mathbf{F}_s(\mathbf{x}, t)$ is calculated by

$$\mathbf{F}_s(\mathbf{x}, t) = \sum_{n=1}^{n_{\max}} \mathbf{F}_s^n(\mathbf{x}, t). \quad (28)$$

After obtaining the IB-induced force term $\mathbf{F}_s(\mathbf{x}, t)$ and the corrected velocity $\mathbf{u}(\mathbf{x}, t)$ on the Eulerian grid, the evolution of $f_i(\mathbf{x}, t)$ will move to time step $t + \delta_t$.

The above description explains the conventional IB-LB method. Subsequently, the IB-LB method for REV-scale incompressible flows will be described in detail. Analogizing with Eq. (14) in the conventional IB-LB method, the REV-scale intermediate velocity $\mathbf{u}^*(\mathbf{x}, t)$ and corresponding correction $\delta\mathbf{u}(\mathbf{x}, t)$ can be expressed as

$$\mathbf{u}(\mathbf{x}, t) = \mathbf{u}^*(\mathbf{x}, t) + \delta\mathbf{u}(\mathbf{x}, t), \quad (29)$$

$$\mathbf{u}^*(\mathbf{x}, t) = \frac{1}{\rho(\mathbf{x}, t)} \sum_i \mathbf{e}_i f_i(\mathbf{x}, t) + \frac{\delta_t}{2} \mathbf{F}_b[\mathbf{u}^*(\mathbf{x}, t)], \quad (30)$$

$$\delta\mathbf{u}(\mathbf{x}, t) = \frac{\delta_t}{2} \left\{ \mathbf{F}_b[\mathbf{u}(\mathbf{x}, t)] - \mathbf{F}_b[\mathbf{u}^*(\mathbf{x}, t)] + \mathbf{F}_s(\mathbf{x}, t) \right\}. \quad (31)$$

Due to the existence of the quadratic force term $\mathbf{F}_b[\mathbf{u}(\mathbf{x}, t)]$ in Eq. (31), the relation between IB-induced force term $\mathbf{F}_s(\mathbf{x}, t)$ and velocity correction $\delta\mathbf{u}(\mathbf{x}, t)$ is nonlinear. The $\delta\mathbf{u}(\mathbf{x}, t)$ is related to both $\mathbf{F}_s(\mathbf{x}, t)$ and $\mathbf{u}(\mathbf{x}, t)$, while $\mathbf{u}(\mathbf{x}, t)$ is derived after correcting $\mathbf{u}^*(\mathbf{x}, t)$ by $\delta\mathbf{u}(\mathbf{x}, t)$. As a result, the force term $\mathbf{F}_s(\mathbf{X}_j, t)$ is unable to be calculated by $\mathbf{u}(\mathbf{X}_j, t)$ and $\mathbf{u}^*(\mathbf{X}_j, t)$ like Eq. (23), and $\mathbf{F}_s(\mathbf{x}, t)$ fails to directly tune the $\delta\mathbf{u}(\mathbf{x}, t)$ like Eq. (22). Thus, the specific velocity $\mathbf{u}(\mathbf{X}_j, t)$ on the IB cannot be implemented by the conventional IB-LB method.

To remove this drawback, the temporary velocity correction-based IB-LB method is established. The main goal is to construct a linear relation between temporary velocity correction $\delta\mathbf{v}(\mathbf{x}, t)$ and the IB-induced force term $\mathbf{F}_s(\mathbf{x}, t)$. Thus, the calculation strategy of the unknown surface force term $\mathbf{f}_s(s_j, t)$ in the conventional IB-LB method can be directly extended to the REV-scale fluid flows in porous media. The specific boundary condition can be enforced based on correcting the temporary velocity. The detailed derivation of the proposed method is demonstrated as follows.

In order to avoid the coupling between $\mathbf{F}_s(\mathbf{x}, t)$ and $\mathbf{u}(\mathbf{x}, t)$, the temporary velocity $\mathbf{v}(\mathbf{x}, t)$ is introduced to construct $\mathbf{F}_s(\mathbf{x}, t)$. Based on Eq. (15), the temporary velocity $\mathbf{v}(\mathbf{x}, t)$ is described as

$$\begin{aligned}\mathbf{v}(\mathbf{x}, t) &= \mathbf{v}^*(\mathbf{x}, t) + \delta\mathbf{v}(\mathbf{x}, t), \\ \mathbf{v}^*(\mathbf{x}, t) &= \frac{1}{\rho(\mathbf{x}, t)} \sum_i \mathbf{e}_i f_i(\mathbf{x}, t), \quad \delta\mathbf{v}(\mathbf{x}, t) = \frac{\delta_t}{2} \mathbf{F}_s(\mathbf{x}, t),\end{aligned}\quad (32)$$

where $\mathbf{v}^*(\mathbf{x}, t)$ is the intermediate temporary velocity and $\delta\mathbf{v}(\mathbf{x}, t)$ is the temporary velocity correction. The linear relation between $\delta\mathbf{v}(\mathbf{x}, t)$ and

$F_s(\mathbf{x}, t)$ is established. $F_s(\mathbf{x}, t)$ can be employed to correct $\mathbf{v}^*(\mathbf{x}, t)$, and the $F_s(\mathbf{x}, t)$ can be obtained through $\delta \mathbf{v}(\mathbf{x}, t)$ directly.

From Eqs. (16) and (17), $\mathbf{u}(\mathbf{x}, t)$ and $\mathbf{v}(\mathbf{x}, t)$ have a one-to-one mapping. Thus, the specific boundary condition of velocity $\mathbf{u}(\mathbf{X}_j, t)$ can be transformed to the temporary velocity $\mathbf{v}(\mathbf{X}_j, t)$. Furthermore, based on the direct-forcing method, the enforcement of specific boundary condition can be converted as

$$F_s(\mathbf{X}_j, t) = \frac{2}{\delta_t} [\mathbf{v}(\mathbf{X}_j, t) - \mathbf{v}^*(\mathbf{X}_j, t)]. \quad (33)$$

In Eq. (33), to obtain the $F_s(\mathbf{X}_j, t)$, the unknown intermediate temporary velocity $\mathbf{v}^*(\mathbf{X}_j, t)$ is converted from $\mathbf{u}^*(\mathbf{X}_j, t)$ by

$$\mathbf{v}^*(\mathbf{X}_j, t) = [2c_0 + c_1 |\mathbf{u}^*(\mathbf{X}_j, t)|] \mathbf{u}^*(\mathbf{X}_j, t), \quad (34)$$

where $\mathbf{u}^*(\mathbf{X}_j, t)$ is interpolated from $\mathbf{u}^*(\mathbf{x}, t)$ through Eq. (24). Additionally, $\mathbf{u}^*(\mathbf{x}, t)$ is transformed from $\mathbf{v}^*(\mathbf{x}, t)$ by

$$\mathbf{u}^*(\mathbf{x}, t) = \mathbf{v}^*(\mathbf{x}, t) / \left[c_0 + \sqrt{c_0^2 + c_1 |\mathbf{v}^*(\mathbf{x}, t)|} \right], \quad (35)$$

where $\mathbf{v}^*(\mathbf{x}, t)$ is calculated through the post-streaming distribution functions $f_i(\mathbf{x}, t)$ based on Eq. (32).

The surface force term $\mathbf{f}_s(s_j, t)$ can be calculated through Eq. (25), which will distribute to the body force term $F_s(\mathbf{x}, t)$ in terms of Eq. (18). Furthermore, the temporary velocity $\mathbf{v}(\mathbf{x}, t)$ is obtained by correcting $\mathbf{v}^*(\mathbf{x}, t)$ based on Eq. (32), and the velocity $\mathbf{u}(\mathbf{x}, t)$ can be transformed from $\mathbf{v}(\mathbf{x}, t)$ through Eq. (16). So far, the temporary velocity correction-based direct-forcing IB-LB method for REV-scale fluid flows is established.

Similarly with the conventional IB-LB method, the specific boundary condition of temporary velocity $\mathbf{v}(\mathbf{X}_j, t)$ cannot be accurately guaranteed in the direct-forcing method. To further obtain the surface force term $\mathbf{f}_s(s_j, t)$ accurately with the enforcement of the specific boundary condition, $\mathbf{f}_s(s_j, t)$ is calculated iteratively during every time step using the multi-direct-forcing scheme,¹⁷ which is expressed as

$$\mathbf{f}_s^n(s_j, t) = \delta_x F_s^n(\mathbf{X}_j, t) = 2\delta_x \frac{\mathbf{v}(\mathbf{X}_j, t) - \mathbf{v}^{*,n-1}(\mathbf{X}_j, t)}{\delta_t}. \quad (36)$$

After spreading $\mathbf{f}_s^n(s_j, t)$ into the Eulerian grid using Eq. (18), $F_s^n(\mathbf{x}, t)$ can be obtained to correct $\mathbf{v}^n(\mathbf{x}, t)$ as

$$\mathbf{v}^{*,n}(\mathbf{x}, t) = \mathbf{v}^{*,n-1}(\mathbf{x}, t) + \frac{1}{2} \delta_t F_s^n(\mathbf{x}, t). \quad (37)$$

The transformation between \mathbf{u} and \mathbf{v} is used during the implementation of the multi-direct-forcing IB-LB method. The $\mathbf{u}^{*,n}(\mathbf{x}, t)$ is calculated through Eq. (35), and the $\mathbf{u}^{*,n}(\mathbf{X}_j, t)$, interpolated from $\mathbf{u}^{*,n}(\mathbf{x}, t)$ using Eq. (25), is converted to $\mathbf{v}^{*,n}(\mathbf{X}_j, t)$ through Eq. (34).

The same convergence criterion with the conventional multi-direct-forcing method is employed. That is when $\mathbf{v}^{*,n}(\mathbf{X}_j, t)$ reaches to the specific boundary condition $\mathbf{v}(\mathbf{X}_j, t)$ or when n reaches the pre-defined maximum iteration number n_{\max} . After finishing the correction of temporary velocity $\mathbf{v}^*(\mathbf{x}, t)$ through Eq. (37), $F_s(\mathbf{x}, t)$ and $\mathbf{u}(\mathbf{x}, t)$ can be computed through Eqs. (16) and (28), respectively.

The iteration procedures on different grids are given in Fig. 2. It shows that in the proposed IB-LB method, the velocity interpolation from Eulerian grid to Lagrangian grid is conducted on $\mathbf{u}^{*,n}(\mathbf{x}, t)$. On the Lagrangian grid, the boundary condition on the IB points is transformed from $\mathbf{u}(\mathbf{X}_j, t)$ to $\mathbf{v}(\mathbf{X}_j, t)$. The surface force term $\mathbf{f}_s^n(s_j, t)$, calculated based on $\mathbf{v}^{*,n}(\mathbf{X}_j, t)$ and $\mathbf{v}(\mathbf{X}_j, t)$, will spread to the $F_s^n(\mathbf{x}, t)$. On the Eulerian grid, the $\mathbf{v}^{*,n}(\mathbf{x}, t)$ is corrected by $F_s^n(s_j, t)$ and will be transformed to the $\mathbf{u}^{*,n}(\mathbf{x}, t)$. After finishing the iteration, the distribution functions are updated by performing the collision and streaming on the Eulerian grid.

The proposed temporary velocity correction-based IB-LB method is reduced to the conventional IB-LB method when neglecting the effect of porous media. Additionally, this method can also be employed to other problems with the velocity-related force term.

C. Implementation procedures

The computation procedures of the proposed IB-LB method are summarized as follows.

- (1) Generate the Eulerian grid and Lagrangian grid, initialize $\rho(\mathbf{x}, t)$, $\mathbf{u}(\mathbf{x}, t)$, $F_s(\mathbf{x}, t)$, and $f_i(\mathbf{x}, t)$, and set $\mathbf{v}(\mathbf{X}_j, t)$ on all the IB points.
- (2) Perform the collision and streaming of density distribution $f_i(\mathbf{x}, t)$ based on Eq. (8) and calculate $\mathbf{v}^*(\mathbf{x}, t)$ and $\mathbf{u}^*(\mathbf{x}, t)$ using Eqs. (32) and (35) [namely, $\mathbf{v}^{*,n-1}(\mathbf{x}, t)$ and $\mathbf{u}^{*,n-1}(\mathbf{x}, t)$ with $n = 1$].
- (3) Obtain $\mathbf{u}^{*,n-1}(\mathbf{X}_j, t)$ using Eq. (24) and compute $\mathbf{v}^{*,n-1}(\mathbf{X}_j, t)$ using Eq. (34). Calculate $\mathbf{f}_s^n(\mathbf{X}_j, t)$ by Eq. (36) and spread $\mathbf{f}_s^n(\mathbf{X}_j, t)$ to Eulerian grid to obtain $F_s^n(\mathbf{x}, t)$ by Eq. (18).
- (4) Correct $\mathbf{v}^{*,n}(\mathbf{x}, t)$ using Eq. (37) and calculate $\mathbf{u}^{*,n}(\mathbf{x}, t)$ using Eq. (35).

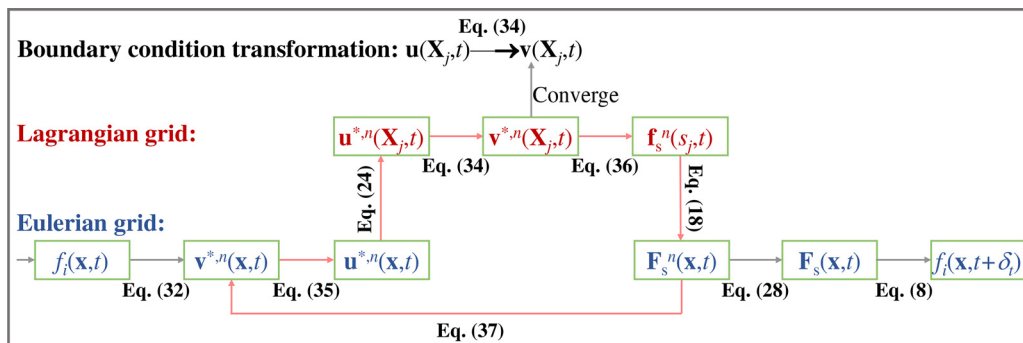


FIG. 2. Iteration procedures (denoted by the red lines) of the proposed IB-LB method.

- (5) Repeat steps (3)–(4) for the $n + 1$ inner iteration until $\mathbf{v}^{*,n}(\mathbf{X}_j, t)$ reach $\mathbf{v}(\mathbf{X}_j, t)$ [namely, $\mathbf{u}^{*,n}(\mathbf{X}_j, t) = \mathbf{u}(\mathbf{X}_j, t)$] or n reaches predefined iteration step n_{\max} , compute $\mathbf{F}_s(\mathbf{x}, t)$ using Eq. (28), and set $\mathbf{u}(\mathbf{x}, t) = \mathbf{u}''(\mathbf{x}, t)$.
- (6) Go back to steps (2)–(5) for the evolution of $f_j(\mathbf{x}, t + \delta_t)$.

III. NUMERICAL EXAMPLES

In this section, some numerical examples are employed to verify the proposed temporary velocity-based IB–LB method for the incompressible flows in porous media. The Couette flow in a porous annulus and the lid driven flow in a square cavity filled with porous matrix are simulated. In all the simulations, $J = 1$, $\delta_x = \delta_t = 1$, IB points are arranged uniformly with $\Delta x = 0.5\delta_x$. To balance the accuracy and computational efficiency, the maximum iteration number n_{\max} equals 5.¹⁷ If not specified, the Forchheimer coefficient F_ε is calculated through Eq. (6).

A. Couette flow in a porous annulus

In this subsection, Couette flow in a porous annulus is employed to verify the proposed IB–LB method.³⁰ As depicted in Fig. 3, the annulus is filled with porous media, and the inner and outer radii of the annulus are R_i and R_o , respectively. The inner wall of the annulus rotates anticlockwise around annulus center with angular velocity ω . The outer wall is stationary. This flow phenomenon is fully two-dimensional, and the IB–LB method is employed to enforce the velocity boundary condition on the inner and outer walls. Due to the symmetry of the geometry and the boundary conditions, the steady velocity field can be simplified as a one-dimensional azimuthal velocity (u_θ) distribution varied with the radial location r , which can be expressed as

$$\frac{\nu_e}{r} \frac{d}{dr} \left(r \frac{du_\theta}{dr} \right) - \frac{\nu_e u_\theta}{r^2} - \frac{\varepsilon \nu}{K} u_\theta - \frac{\varepsilon F_\varepsilon}{\sqrt{K}} u_\theta^2 = 0. \quad (38)$$

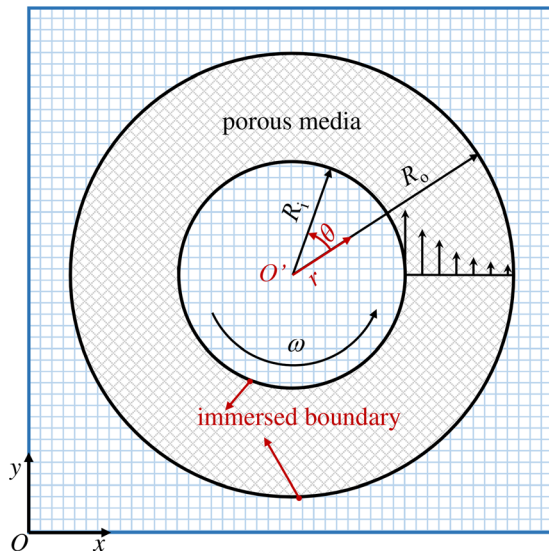


FIG. 3. Schematic diagram of the Couette flow in porous annulus.

The effects of Re , Da , and ε are investigated. Different simulation parameters used in this section are given in Table I. The characteristic length L_c in Re and Da is defined as $R_o - R_i$, and the characteristic velocity u_c in Re is fixed at $R_i \omega$. To ensure the incompressible condition, the dimensionless relaxation time τ equals 0.9, 0.52, and 0.9, respectively, in cases 1, 2, and 3. The characteristic velocity u_c can be determined through the definition of Re . The grid size between inner and outer radii along the radial direction is 90 in the IB–LB simulations. Because the analytical solution of Eq. (38) is difficult to obtain, the results obtained by the finite-difference (FD) method are employed to validate the IB–LB method. To obtain an accurate FD solution, the second-order central difference scheme is used for the space discretization, and the characteristic length L_c is divided into 128 nodes.

Figure 4 illustrates the distributions of u_θ in different cases. As shown in this figure, with the increase in Da in case 1, the effect of porous media decreases, and u_θ/u_c at the same radial location increases gradually. For case 2 at the same Da and ε , the velocity profiles become steeper with the increase in Re . When ε increases from 0.2 to 0.8 in case 3, the same influence tendency on the velocity profile but with a small variation is shown compared with the effect of Da . As can be seen from Fig. 4, the present solutions agree well with those FD solutions. Thus, the proposed IB–LB method can accurately enforce the boundary condition on the IB.

The original LB method has a second-order accuracy in space and time. However, during the enforcement of the specific velocity boundary condition, the first-order Dirac delta function is employed which will affect the overall accuracy. The whole convergence characteristic of the proposed IB–LB method should be further investigated.

To qualify the numerical error, the L_2 norm for the u_r is adopted, which is defined as

$$L_2 - \text{error} = \sqrt{\frac{1}{N} \sum_N \left(\frac{u_r^n}{u_r^a} - \frac{u_r^a}{u_r^a} \right)^2}, \quad (39)$$

where the subscripts n and a denote the numerical and analytical solutions and N is the total Eulerian grid points inside the physical domain. In this test, the numerical results with the refined grid are used as u_r^a . The simulation parameters are set as $Re = 10$, $Da = 0.1$, $\varepsilon = 0.9$, and $\tau = 0.9$. The characteristic length L_c is discretized into $n = 30, 60$, and 120 grid points. The grid for refined solution u_r^a is set

TABLE I. Parameters used in Couette flow simulations.

	Simulation parameters			
	Re	Da	ε	τ
Case 1	10	0.001 0.01 0.1	0.9	0.9
Case 2	0.1 100 1000	0.1	0.9	0.52
Case 3	10	0.1	0.2 0.5 0.8	0.9

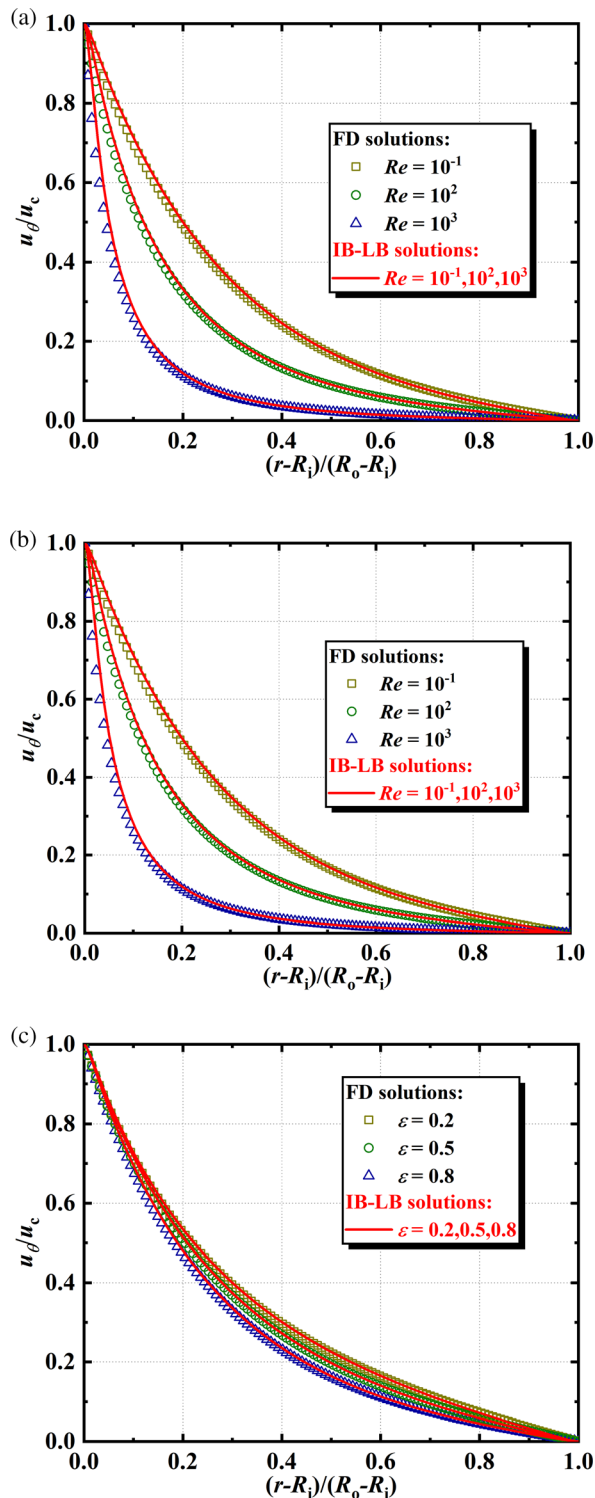


FIG. 4. Velocity distributions of the Couette flow in a porous annulus. (a) case 1, (b) case 2, and (c) case 3; (a) case 1: $Re = 10$, $\varepsilon = 0.9$; (b) case 2: $Da = 0.1$, $\varepsilon = 0.9$; and (c) case 3: $Re = 10$, $Da = 0.1$.

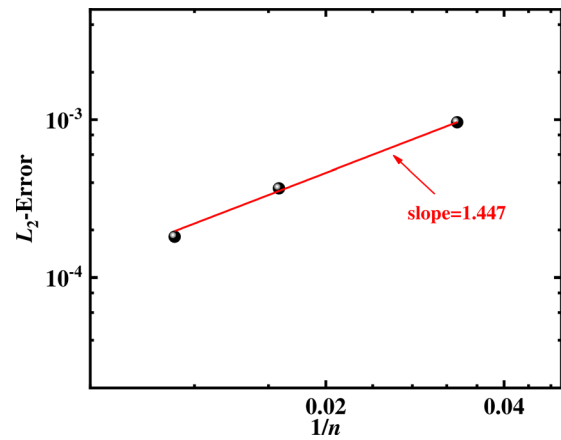


FIG. 5. The L_2 -norm numerical errors of u_r at different grid sizes.

as $n = 240$ grid points on L_c . The numerical results of L_2 -error are given in Fig. 5. As shown in this figure, the numerical convergence rate is less than the original LB method due to the numerical error caused by the interpolation function during the treatment of the boundary condition.

B. Lid driven flow in a square porous cavity

Lid driven flow is widely employed as the benchmark case for different numerical methods.^{11,31,32} The lid driven flow in a square cavity filled with porous matrix is investigated here for the verification of the proposed temporary velocity correction-based IB-LB method.

In the most of previous simulations, the walls of cavity are parallel with grid, so the regular velocity boundary condition can be easily implemented.^{11,33} To show the numerical performance of the proposed IB-LB method, an inclined cavity intersected with the Eulerian

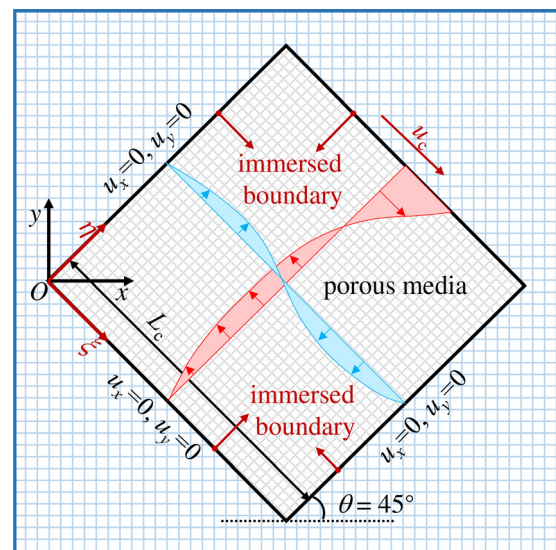


FIG. 6. Schematic diagram of lid driven flow in a square porous cavity.

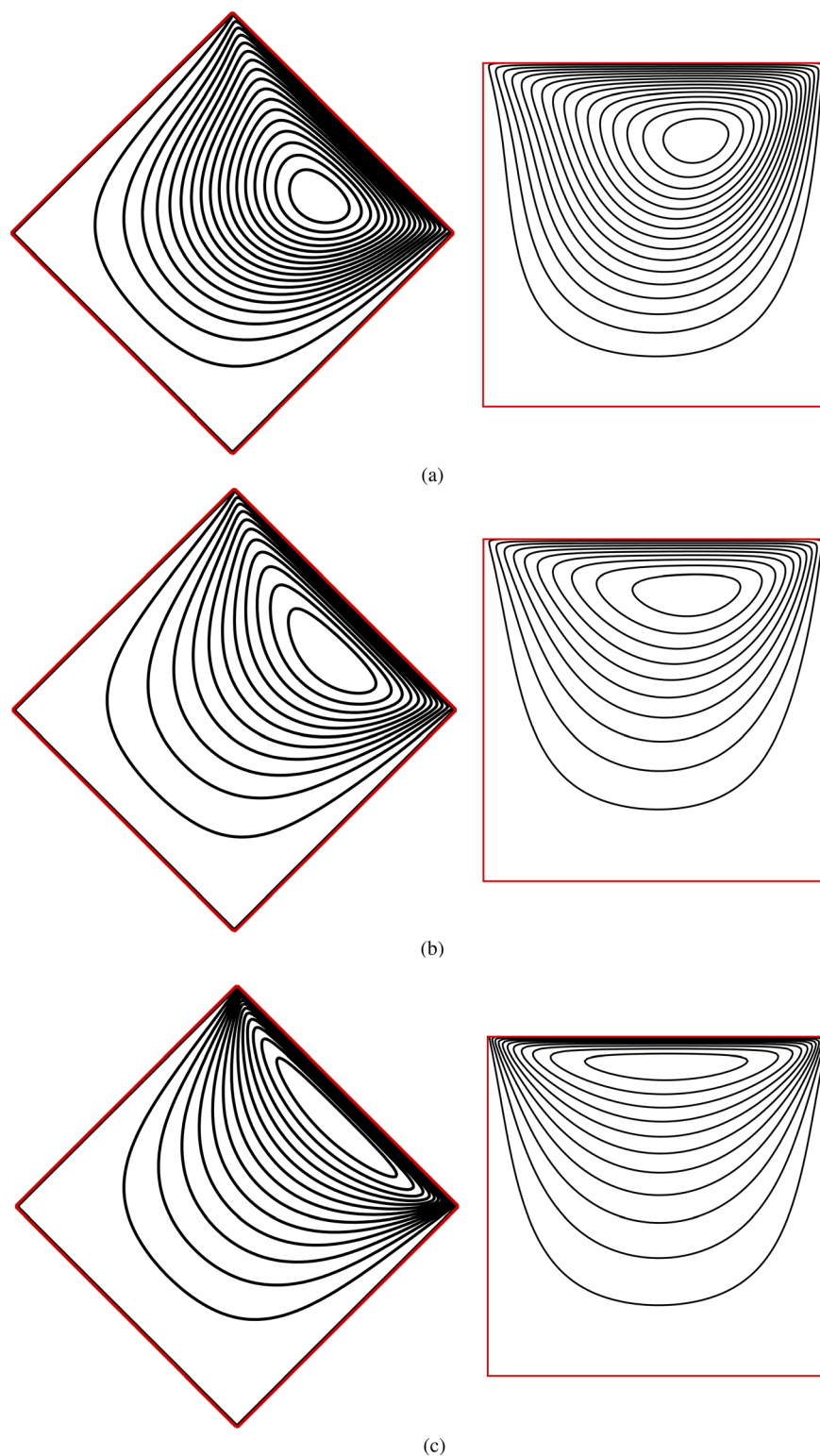


FIG. 7. Streamlines of lid driven flows at different Da (left: results by the proposed IB-LB method, right: results by the LB method). (a) $Da = 10^{-2}$, (b) $Da = 10^{-3}$, and (c) $Da = 10^{-4}$.

grid is simulated, while the boundary condition on the inclined walls is enforced by the proposed IB-LB method. The sketch of this numerical case is given in Fig. 6. In the xoy coordinate system, a square porous cavity is anti-clockwise inclined by 45° , and the length of side walls is L_c . The moving velocity of the driven lid is u_c , and other walls are stationary. In order to simplify the presentation, another coordinate system $\xi O\eta$ is introduced by rotating the original xoy system 45° clockwise. The cavity is located at $0 \leq \xi \leq L_c$ and $0 \leq \eta \leq L_c$. The uniform Eulerian grid is arranged along the xoy coordinate axes, while the walls of cavity are parallel with the inclined $\xi O\eta$ system. The simulation parameters are set as $\varepsilon = 0.1$, $Re = 10$, and $Da = 0.01, 0.001$, and 0.0001 . The dimensionless relaxation time τ equals 0.8 . Two sets of Eulerian grids with $N_\xi \times N_\eta = 100 \sqrt{2} \times 100 \sqrt{2}$ (coarse grid) and $150 \sqrt{2} \times 150 \sqrt{2}$ (fine grid) are used.

For comparison, the simulation results in Ref. 11 are used to show the accuracy of the proposed IB-LB method. However, only the velocity profiles were given in the original work. Due to the distribution of streamlines is an important parameter for the numerical

studies, to further show this characteristic, the standard LB simulation based on Ref. 11 is carried out in the $\xi O\eta$ system. The halfway bounce-back scheme is employed to treat the straight boundary condition parallel with the grid.³⁴

The streamlines at different Da numbers are shown in Fig. 7. Different sets of grids obtain almost the same results. When the Da number (i.e., permeability K) is small, the flow is weak due to the effect of porous media. With the increase in Da number, the flows are enhanced, and the vortexes move to the cavity center. Numerical results obtained by different methods are almost the same. To further show the accuracy of the IB-LB method, the velocity profiles of u_ξ at $\eta/L_c = 0.5$ and u_η at $\xi/L_c = 0.5$ are given in Fig. 8. The velocity profiles with different grids at different Da numbers agree well with both the present standard LB solutions and those in Ref. 11. Therefore, the temporary velocity correction-based IB-LB method can predict the incompressible flow fields in porous media accurately.

IV. CONCLUSIONS

An IB-LB method is proposed for incompressible flows through porous media at the REV scale. In the proposed method, the temporary velocity is introduced, which can be decomposed into the intermediate temporary velocity and temporary velocity correction. As a result, a linear relation between the force term accounting for the IB and temporary velocity correction is constructed. Furthermore, to obtain the IB-induced force term with the enforcement of the specific boundary condition, the boundary condition of velocity is transformed to temporary velocity. Compared with the conventional IB-LB method, the coupling between the force term induced by the porous media and velocity can be overcome. To avoid the error introduced by the explicit calculation of force term as the conventional IB-LB method, the multi-direct-forcing scheme is employed for calculating force term iteratively. The specific boundary condition can be enforced accurately. Couette flow in a porous annulus and lid driven flow in a square cavity filled with porous matrix are employed for validation. Numerical results show the accuracy of the IB-LB method. This method can be also applied for other models with the velocity-related force terms.

ACKNOWLEDGMENTS

This work was supported by the Basic Science Center Program for Ordered Energy Conversion of the National Natural Science Foundation of China (No. 51888103) and the National Natural Science Foundation of China (No. 51906186).

The authors would also like to thank the Foundation for Innovative Research Groups of the National Natural Science Foundation of China (No. 51721004).

AUTHOR DECLARATIONS

Conflict of Interest

The authors have no conflicts to disclose.

DATA AVAILABILITY

The data that support the findings of this study are available from the corresponding author upon reasonable request.

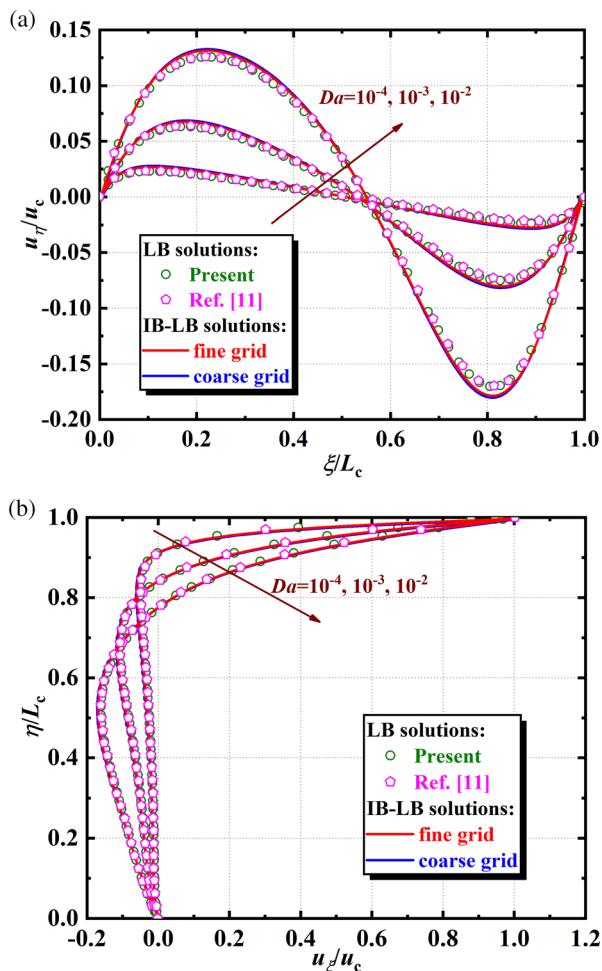


FIG. 8. Velocity profiles of lid driven flows at different Da . (a) u_η vs ξ and (b) u_ξ vs η .

REFERENCES

- ¹S. Rashidi, J. A. Esfahani, and N. Karimi, "Porous materials in building energy technologies—A review of the applications, modelling and experiments," *Renewable Sustainable Energy Rev.* **91**, 229–247 (2018).
- ²L. Germanou, M. T. Ho, Y. H. Zhang, and L. Wu, "Shale gas permeability upscaling from the pore-scale," *Phys. Fluids* **32**, 102012 (2020).
- ³S. Zhang, D. L. Feng, L. Shi, L. Wang, Y. G. Jin, L. M. Tian, Z. Y. Li, G. Y. Wang, L. Zhao, and Y. Y. Yan, "A review of phase change heat transfer in shape-stabilized phase change materials (ss-PCMs) based on porous supports for thermal energy storage," *Renewable Sustainable Energy Rev.* **135**, 110127 (2021).
- ⁴D. A. Nield and A. Bejan, *Convection in Porous Media* (Springer, 2006).
- ⁵Y. Xu, Q. L. Ren, Z. J. Zheng, and Y. L. He, "Evaluation and optimization of melting performance for a latent heat thermal energy storage unit partially filled with porous media," *Appl. Energy* **193**, 84–95 (2017).
- ⁶B. M. Shankar and I. S. Shivakumara, "Changes in the hydrodynamic stability of plane porous-Couette flow due to vertical throughflow," *Phys. Fluids* **33**, 074103 (2021).
- ⁷S. Chen and G. D. Doolen, "Lattice Boltzmann method for fluid flows," *Annu. Rev. Fluid Mech.* **30**, 329–364 (1998).
- ⁸X. He and L.-S. Luo, "A priori derivation of the lattice Boltzmann equation," *Phys. Rev. E* **55**, R6333 (1997).
- ⁹T. Krüger, H. Kusumaatmaja, A. Kuzmin, O. Shardt, G. Silva, and E. M. Viggien, *The Lattice Boltzmann Method* (Springer, 2017).
- ¹⁰Y. L. He, Y. Wang, and Q. Li, *Lattice Boltzmann Method: Theory and Applications* (Science Press, Beijing, 2009).
- ¹¹Z. L. Guo and T. S. Zhao, "Lattice Boltzmann model for incompressible flows through porous media," *Phys. Rev. E* **66**, 036304 (2002).
- ¹²Y. L. He, Q. Liu, Q. Li, and W. Q. Tao, "Lattice Boltzmann methods for single-phase and solid-liquid phase-change heat transfer in porous media: A review," *Int. J. Heat Mass Transfer* **129**, 160–197 (2019).
- ¹³G. Kefayati, A. Tolooiyan, A. P. Bassom, and K. Vafai, "A mesoscopic model for thermal-solutal problems of power-law fluids through porous media," *Phys. Fluids* **33**, 033114 (2021).
- ¹⁴G. Kefayati, "Lattice Boltzmann simulation of double-diffusive natural convection of viscoplastic fluids in a porous cavity," *Phys. Fluids* **31**, 013105 (2019).
- ¹⁵C. S. Peskin, "Flow patterns around heart valves: A numerical method," *J. Comput. Phys.* **10**, 252–271 (1972).
- ¹⁶Z. G. Feng and E. E. Michaelides, "The immersed boundary-lattice Boltzmann method for solving fluid-particles interaction problems," *J. Comput. Phys.* **195**, 602–628 (2004).
- ¹⁷S. K. Kang and Y. A. Hassan, "A comparative study of direct-forcing immersed boundary-lattice Boltzmann methods for stationary complex boundaries," *Int. J. Numer. Methods Fluids* **66**, 1132–1158 (2011).
- ¹⁸Z. G. Feng and E. E. Michaelides, "Proteus: A direct forcing method in the simulations of particulate flows," *J. Comput. Phys.* **202**, 20–51 (2005).
- ¹⁹X. D. Niu, C. Shu, Y. T. Chew, and Y. Peng, "A momentum exchange-based immersed boundary-lattice Boltzmann method for simulating incompressible viscous flows," *Phys. Lett. A* **354**, 173–182 (2006).
- ²⁰X. He, Q. Zou, L.-S. Luo, and M. Dembo, "Analytic solutions of simple flows and analysis of nonslip boundary conditions for the lattice Boltzmann BGK model," *J. Stat. Phys.* **87**, 115–136 (1997).
- ²¹L.-S. Luo, "Theory of the lattice Boltzmann method: Lattice Boltzmann models for nonideal gases," *Phys. Rev. E* **62**, 4982 (2000).
- ²²Z. L. Guo, C. G. Zheng, and B. C. Shi, "Discrete lattice effects on the forcing term in the lattice Boltzmann method," *Phys. Rev. E* **65**, 046308 (2002).
- ²³X. He, X. Shan, and G. D. Doolen, "Discrete Boltzmann equation model for nonideal gases," *Phys. Rev. E* **57**, R13 (1998).
- ²⁴J. Wu and C. Shu, "Implicit velocity correction-based immersed boundary-lattice Boltzmann method and its applications," *J. Comput. Phys.* **228**, 1963–1979 (2009).
- ²⁵P. Nithiarasu, K. N. Seetharamu, and T. Sundararajan, "Natural convective heat transfer in a fluid saturated variable porosity medium," *Int. J. Heat Mass Transfer* **40**, 3955–3967 (1997).
- ²⁶K. Vafai, "Convective flow and heat transfer in variable-porosity media," *J. Fluid Mech.* **147**, 233–259 (1984).
- ²⁷Y.-H. Qian, D. D'huïères, and P. Lallemand, "Lattice BGK models for Navier-Stokes equation," *Europhys. Lett.* **17**, 479 (1992).
- ²⁸M.-C. Lai and C. S. Peskin, "An immersed boundary method with formal second-order accuracy and reduced numerical viscosity," *J. Comput. Phys.* **160**, 705–719 (2000).
- ²⁹R. Z. Huang and H. Y. Wu, "An immersed boundary-thermal lattice Boltzmann method for solid-liquid phase change," *J. Comput. Phys.* **277**, 305–319 (2014).
- ³⁰Y. Hu, D. Li, S. Shu, and X. Niu, "Finite-volume method with lattice Boltzmann flux scheme for incompressible porous media flow at the representative-elementary-volume scale," *Phys. Rev. E* **93**, 023308 (2016).
- ³¹D.-J. Chen, K.-H. Lin, and C.-A. Lin, "Immersed boundary method based lattice Boltzmann method to simulate 2D and 3D complex geometry flows," *Int. J. Mod. Phys. C* **18**, 585–594 (2007).
- ³²U. Ghia, K. N. Ghia, and C. Shin, "High-Re solutions for incompressible flow using the Navier-Stokes equations and a multigrid method," *J. Comput. Phys.* **48**, 387–411 (1982).
- ³³Q. Liu and Y. L. He, "Multiple-relaxation-time lattice Boltzmann modeling of incompressible flows in porous media," *Phys. A* **429**, 215–230 (2015).
- ³⁴A. J. Ladd, "Numerical simulations of particulate suspensions via a discretized Boltzmann equation. Part 1. Theoretical foundation," *J. Fluid Mech.* **271**, 285–309 (1994).